Journal of Materials Chemistry A

Pressure-induced water producing using a copper–chromium Prussian blue analog

Journal:	*Journal of Materials Chemistry A*
Manuscript ID	TA-ART-11-2024-008305.R1
Article Type:	Paper
Date Submitted by the Author:	01-Apr-2025
Complete List of Authors:	Akagi, Shintaro; University of Tsukuba, Department of Materials Science, Institute of Pure and Applied Sciences Tanaka, Mayuko; University of Tsukuba, Department of Materials Science, Institute of Pure and Applied Sciences Wang, Junhao; University of Tsukuba, Department of Materials Science, Institute of Pure and Applied Sciences Kiuchi, Hisao; The University of Tokyo, Institute for Solid State Physics Harada, Yoshihisa; The University of Tokyo Chen, Yizhou; University of Tsukuba, Department of Materials Science, Institute of Pure and Applied Sciences Marumoto, Kazuhiro; University of Tsukuba, Department of Materials Science, Institute of Pure and Applied Sciences Imoto, Kenta; The University of Tokyo, Department of Chemistry, School of Science, Ohkoshi, Shin-ichi; The University of Tokyo, Department of Chemistry, School of Science Tokoro, Hiroko; University of Tsukuba,

COMMUNICATION

Pressure-induced water producing using a copper–chromium Prussian blue analog

Received 00th January 20xx,
Accepted 00th January 20xx

DOI: 10.1039/x0xx00000x

Shintaro Akagi,[a,§] Mayuko Tanaka,[a,§] Junhao Wang,[a] Hisao Kiuchi,[b] Yoshihisa Harada,[b] Yizhou Chen,[a] Kazuhiro Marumoto,[a] Kenta Imoto,[c] Shin-ichi Ohkoshi,[c,*] Hiroko Tokoro[a,c,*]

To solve the deterioration of water resource environment, on-site water production technologies have garnered attention. Here, we demonstrate the example of pressure-induced water production using a copper–chromium Prussian blue analog (CuCr PBA). Applying pressure caused water droplets to generate from the CuCr PBA. Collecting the water droplets with a pipette revealed that approximately 240 g of water was obtained per 1 kg of CuCr PBA. One possible mechanism of the water production could be the hydrophobization of pores at defect sites based on partial electron transfer from the oxygen of ligand water to copper upon pressure application. This article presents a new approach to water production, which is an important step towards the further development of the water environmental improvement technology.

Introduction

Research on controlling the states and physical properties of solid materials through external stimuli, such as light, pressure, and temperature, has been actively conducted. Cyano-bridged metal complexes have garnered considerable attention as materials exhibiting various external stimulus-responsive functionalities.[1–5] Among cyano-bridged metal complexes, Prussian blue analogs (PBAs), which are hexacyanometallic complexes, have recently become highly regarded materials, with reported various properties including gas storage,[6] proton conductivity,[7] magnetic functionality,[8–13] catalytic properties,[14] and battery characteristic.[15–24] PBAs are widely used in modern society due to their excellent chemical stability and low synthetic cost. [25–30] They are commonly used as pigments and have been used for radioactive cesium recovery,[31,32,] ammonia adsorption,[33] and electrochromical applications.[34,35] PBAs have two types of crystal structures: 1:1:1 and vacancy types. The 1:1:1 type can incorporate alkali cations into its cubic framework, exhibit battery characteristics, and recover cations such as cesium.[26] The vacancy type forms when alkali cations are not included, and the structure contains lattice defects to maintain charge balance. Pores that can capture water molecules exist at these lattice defects.[36–38]

Recently, water scarcity has become a serious problem, especially for people living in arid regions. In contrast to coastal areas, which can use water purification technologies, inland areas require onsite water production technologies to address this problem. Various studies have reported the production of water using hard porous materials, such as zeolites, silica gels, and metal–organic frameworks.[39–43] However, such porous materials require environmental controls to generate water droplets, such as temperature and/or humidity differences.

In this study, we report a copper–chromium PBA (CuCr PBA) that produces water droplets upon pressure application without any temperature or humidity differences. The presence of water molecules in CuCr PBA was investigated using Infrared (IR) spectroscopy and X-ray diffractometry (XRD), and the mechanism of release of water molecules was studied by X-ray absorption and emission spectroscopy.

Results and Discussion

Material

CuCr PBA was prepared by adding 50 cm^{-3} of an aqueous solution of $CuCl_2$ (45 mmol dm^{-3}) to 50 cm^{-3} of an aqueous solution of $K_3[Cr(CN)_6]$ (30 mmol dm^{-3}), which yielded a green powder. Elemental analysis of the obtained powder revealed a formula of $Cu_{1.5}[Cr(CN)_6]\cdot 6.4H_2O$ at 26°C and 27% relative humidity (RH)

[a] Department of Materials Science, Institute of Pure and Applied Sciences, University of Tsukuba, 1-1-1 Tennodai, Tsukuba, Ibaraki 305-8573, Japan
[b] Institute for Solid State Physics (ISSP), The University of Tokyo, 5-1-5, Kashiwanoha, Kashiwa, Chiba 277-8581, Japan
[c] Department of Chemistry, School of Science, The University of Tokyo, 7-3-1 Hongo, Bunkyo-ku, Tokyo 113-0033, Japan
§ These authors contributed equally.

Electronic supplementary information (ESI) available: Detail of physical measurements, crystallographic data, extrapolated curves for the IR Spectra, variation in water content depending on the humidity, IR spectra of silicon dioxide, and IR spectra after pressure application for XES and XAS measurements.
See DOI: 10.1039/x0xx00000x

(calculated: Cu, 22.76; Cr, 12.41; C, 17.20; N, 20.07; H, 3.08%; found: Cu, 23.06; Cr, 12.58; C, 17.36; N, 20.18; H, 2.74%). Powder X-ray diffraction (PXRD) at room temperature revealed a cubic crystal structure (space group: $Fm\bar{3}m$) with a lattice constant of 10.3810(2) Å (Fig. 1a, Table S1a). The cubic structure comprised a framework bridged by cyanide ligands between Cu and Cr (Fig. 1b). The ratio of $Cr(CN)_6$ to Cu was 2:3, and defects were present at one-third of the $Cr(CN)_6$ positions (i.e., existence ratio of $Cr(CN)_6$:defect = 2:1). Water molecules existed in two forms: ligand water in which oxygen was coordinated to Cu at the defect sites [O(1) in Fig. 1c] and lattice water at vacancies [O(2) and O(3) in Fig. 1c].

Water Production

Applying a uniaxial pressure of 1 GPa to a CuCr PBA powder sample at 24°C and 56% RH caused water droplets to emanate from the sample (Fig. 2, Figs. S1–S3 and Supporting Information §5 and §6). The sample became visibly wet and was thoroughly soaked with water droplets. The water expelled from the sample was separated, collected, and quantified over 10 experimental trials, resulting in an average of 3.2 ± 0.4 mg of water per 13.5 mg of sample. These findings indicate that approximately 240 ± 30 g of water can be extracted from 1 kg of CuCr PBA through the application of pressure. IR spectra measured at 25°C and 47% RH before pressure application showed a broad peak in the range of 2500–3800 cm^{-1}, which was attributed to the OH bond of water molecules (Fig. 3, black). After pressure application, the intensity of this peak decreased drastically [Fig. 3 (red), Figs. S4 and S5]. We also observed peaks at 2180 and 2115 cm^{-1} in the IR spectrum prior to pressure application, which we attributed to the CN stretching frequency bridged to Cu and Cr ions (Fig. 3, black). After pressure application (Fig. 3, red), the intensity of the peak at 2115 cm^{-1} increased while the intensity of the peak at 2180 cm^{-1} decreased. This change suggests that the pressure application modified the Cu–NC–Cr bonding state. Possible origins for this change include linkage isomerism of the CN ligand[44–49] (Cu–NC–Cr → Cu–CN–Cr) or a charge transfer between Cu and Cr.

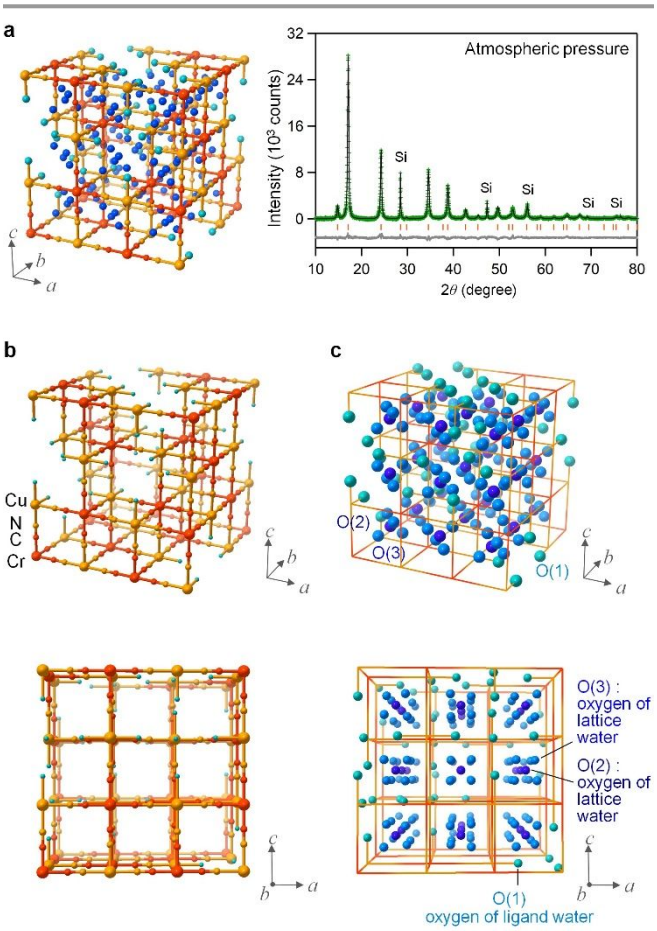

Fig. 1 Crystal structure of CuCr PBA. (a) Crystal structure, XRD pattern, and Rietveld analysis of CuCr PBA under atmospheric pressure. The green dots, black lines, and gray dots represent the observed plots, calculated patterns, and their differences, respectively. The orange bars represent the calculated positions of the Bragg reflections for the CuCr PBA cubic structure. Si powder was used as a standard sample to calibrate the XRD patterns. The crystal structure was cubic, which is common for vacancy-type PBAs. (b) Illustration of the cubic framework comprising Cu and Cr bridged by CN. (c) Illustration of oxygen in water molecules positioned in the cubic framework. O(1) indicates oxygen of ligand water coordinated to copper, O(2) indicates oxygen of lattice water located at the center of vacancy, and O(3) indicates oxygen located around the center of vacancy. For clarity, a cubic structure with defects is shown. In Table S1a, lattice defects are indicated as atomic occupancy.

Hydrogen Bonding of Water Molecules and Valence States of Metal Ions

We investigated the hydrogen bonding in the water molecules using soft X-ray absorption (XAS) and emission spectroscopy (XES) by using synchrotron radiation. Figure 4a shows the O 1s (K-edge) XES spectra of the water molecules before and after the application of 2 GPa of pressure. A broad XES signal was observed around 520–530 eV, which reflects the hydrogen-bonded water molecules. The intensity of the XES signal decreased after pressure application, indicating that some water molecules were pushed out of the material by pressure. Figure 4b shows the O 1s (K-edge) XAS spectrum of the water molecules. Similar to the O 1s XES results, the decrease in the XAS intensity around 534–550 eV after pressure application was ascribed to the pressure-induced water expulsion from the material. In contrast, in the energy region of 530–534 eV, an absorption peak appeared, which suggests that altered coordination emerges in the water molecules after pressure application. Considering that there is no absorption peak below 533 eV in the XAS spectrum of pure water,[50] we attributed the emerging peak to the formation of O 2p–Cu 3d hybrid orbitals between the oxygen of ligand water molecules and the hydrated copper at defect sites, which would induce partial electron transfer from oxygen to copper.

Next, we investigated the valence state of the metal ions. Figure 4c shows the Cu 2p (L3-edge) XAS spectrum. Before pressure application, a strong peak was observed at 931 eV and a weak peak was observed at 936.5 eV. Both peaks indicated that the valence state of copper was Cu(II) because the peak position for Cu(I) is 933.7 eV.[51,52] After pressure application, the peak intensity at 931 eV decreased and the

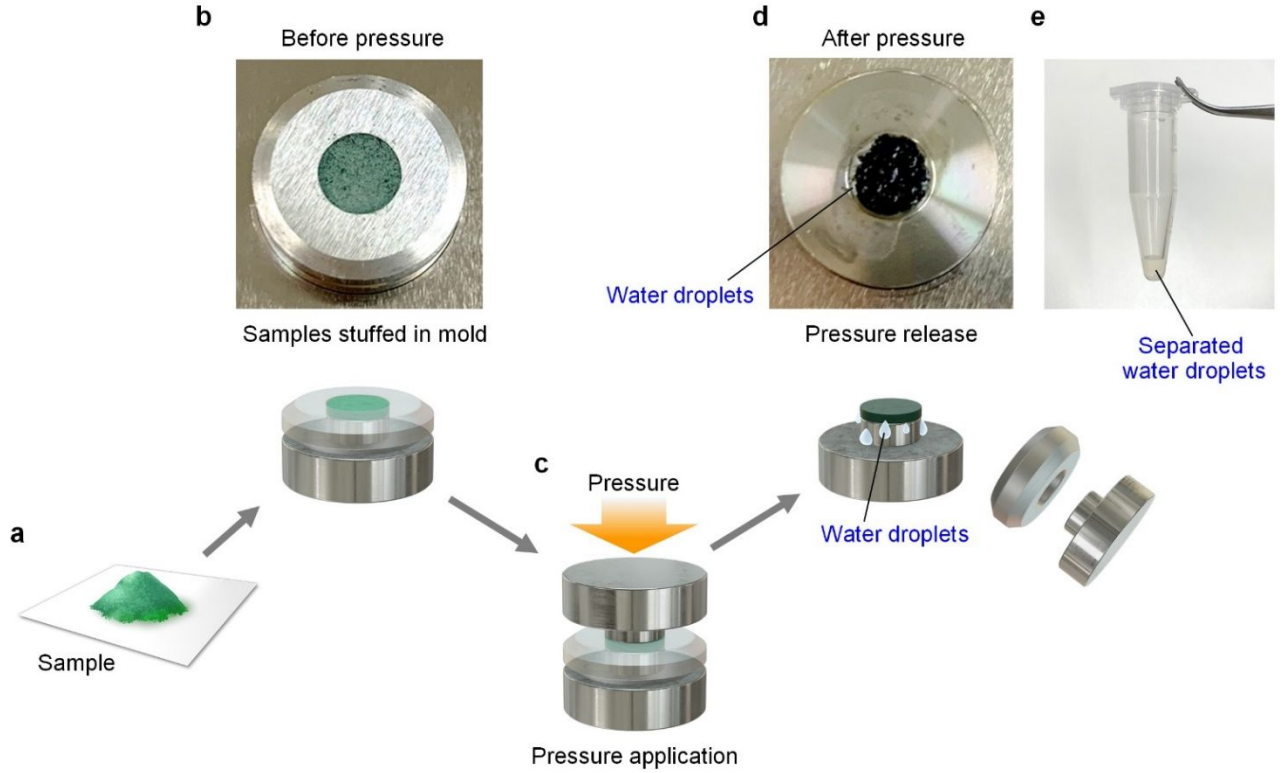

Fig. 2 Pressure-induced water production by the CuCr PBA. Powder samples (a) were placed into molds (b). A uniaxial pressure of 1 GPa was applied for 10 min to the sample (c). Upon release of the pressure, water was expelled out from the sample (d). The photographs were captured from above the sample. The expelled water was subsequently collected and separated (e).

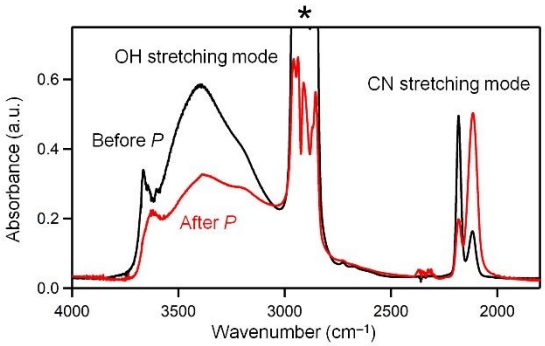

Fig. 3 IR spectra before (black line) and after (red line) pressure application of 2 GPa. The region marked by the asterisk (3050–2750 cm^{-1}) indicates the signal from liquid paraffin.

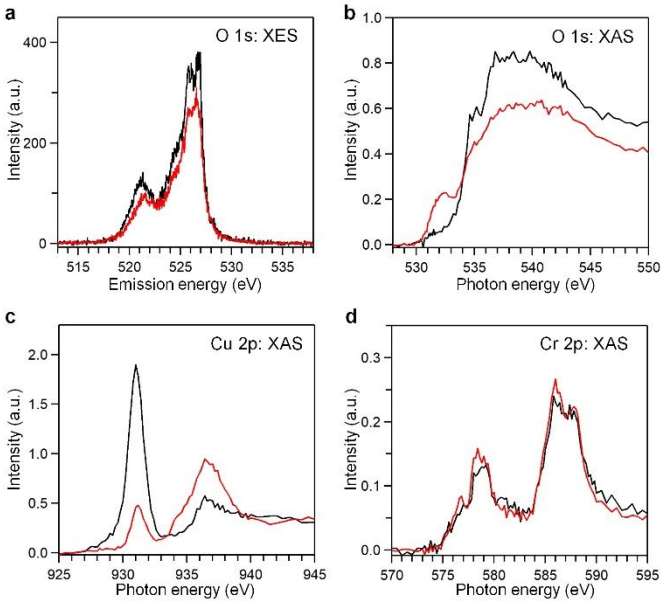

Fig. 4 XES and XAS spectra of the CuCr PBA before (black line) and after (red line) pressure application. (a) XES spectra for O (1s) of water molecules. (b) XAS spectra for O (1s) of water molecules. (c) XAS spectra for Cu (2p). (d) XAS spectra for Cr (2p).

peak intensity at 936.5 eV increased. These changes reflected the partial electron transfer from oxygen to copper due to the formation of O 2p–Cu 3d hybrid orbitals, as observed in the O 1s XAS spectrum (Fig. 4b). Figure 4d shows the Cr 2p (L-edge) XAS spectra with peaks observed at 578.5, 586, and 588 eV. The spectra did not change significantly before and after pressure application, which indicates that the valence state of chromium remained at Cr(III) regardless of pressure.

Cubic Framework and Water Molecules after Pressure

Finally, we investigated the crystallographic changes induced by pressure. The XRD patterns before and after pressure application revealed no drastic changes in the diffraction peak positions and intensity ratios, which indicates that the CuCr PBA maintained its cubic framework (Fig. 5a). The lattice constant after pressure application was 10.378 Å, which was a 0.03% contraction from the lattice constant of 10.381 Å before

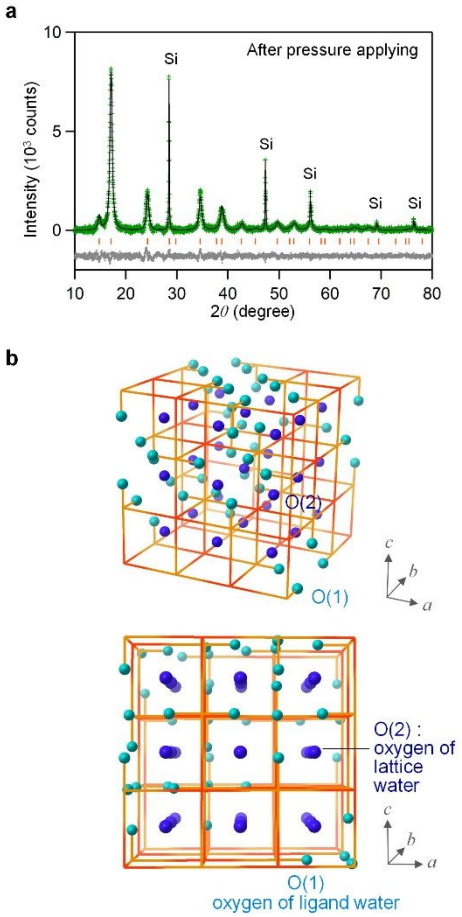

Fig. 5 (a) XRD pattern and Rietveld analysis after application of 2 GPa of pressure. The green dots, black lines, and gray dots represent the observed plots, calculated pattern, and their difference, respectively. The orange bars represent the calculated positions of the Bragg reflections for the CuCr PBA cubic structure. Si powder was used as a standard sample to calibrate the XRD patterns. (b) Illustration of the cubic framework and the oxygen of water. For clarity, a cubic structure with defects is shown. In Table S1b, lattice defects are indicated as atomic occupancy.

pressure application (Table S1b). Regarding the oxygen of water molecules in the crystal structure, Rietveld analyses suggested that the oxygens of the ligand water and lattice water of O(2), located at the center of vacancy, were still present, but the oxygen of the lattice water of O(3), located around the center of vacancy, was absent after pressure application (Fig. 5b).

Mechanism of Pressure-Induced Water Emitting

Based on the measurements before and after pressure application, several insights were obtained: (i) The CuCr PBA generates water droplets upon pressure application. (ii) The CuCr PBA maintains its cubic framework before and after pressure application. (iii) Pressure application expels lattice water located around the center of vacancy, while ligand water and lattice water located at the center of vacancy remains. (iv) Pressure application causes partial electron transfer from the oxygen of the ligand water to copper. (v) Pressure application changes the Cu–NC–Cr bonding state, but the valence states of Cu and Cr remain unchanged. Based on these insights, we proposed the following mechanism for the pressure-induced water producing of CuCr PBA (Fig. 6). Pressure application strengthens the interaction between copper and the oxygen of ligand water molecules, which induces a partial electron transfer from oxygen to copper. This decreases the electron density around the oxygen of the ligand water, which in turn decreases the polarization of the ligand water. The hydrogen bond between the ligand water and neighboring lattice water weakens, and the lattice water is removed from the crystal. The pressure-induced hydrophobization of the originally hydrophilic pores at lattice defect sites may explain the expulsion of lattice water from the crystal. The changes in the IR spectra of the CN stretching frequency can be attributed to the linkage isomerism of the cyanide group because the valence states of Cu and Cr remained unchanged by pressure application.

Conclusions

In this study, we demonstrated the production of water droplets by applying pressure on CuCr PBA. We propose that the hydrophobization of pores at defect sites due to partial electron transfer from the oxygen of ligand water to copper during pressure application is a possible mechanism of pressure-induced water production. The electron transfer is

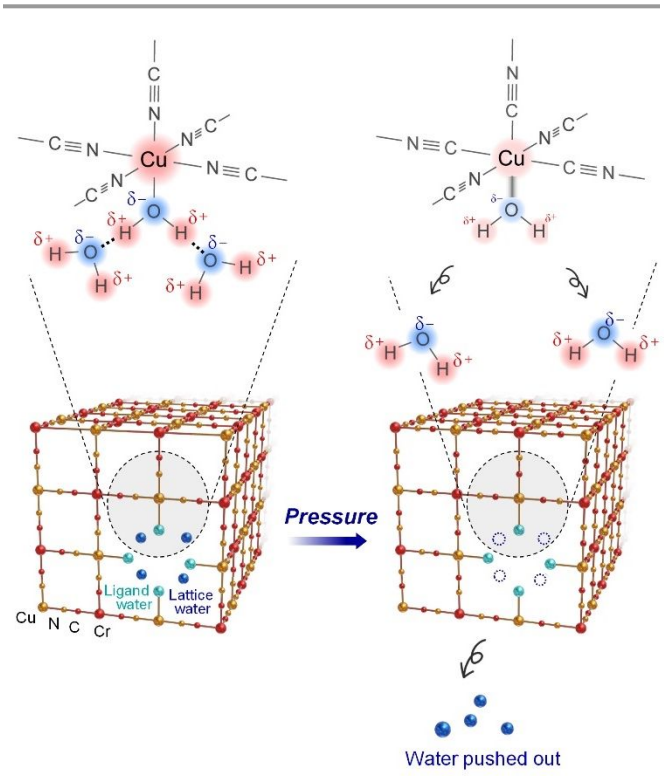

Fig. 6 Schematic illustration of the proposed mechanism for the pressure-induced water production of the CuCr PBA. Pressure application induces a partial electron transfer from oxygen to copper. The electron density around the oxygen of the ligand water decreases, which decreases the polarization of the ligand water. The hydrogen bond between the ligand water and neighboring lattice water weakens, and the lattice water is pushed out of the crystal.

interpreted as inducing cyanide linkage isomerism. To gain further insight into the phenomenon of pressure-induced water production, we investigated whether PBAs other than the CuCr PBA would exhibit similar behaviour. Nine reference PBA samples containing $Cr(CN)_6$ or $Co(CN)_6$ were synthesised and examined (Figs. S6–S9, Tables S3 and S4, and Supporting Information, §9). The results indicated that neither the amount of water encapsulated in the samples nor the particle size correlated with water production. Furthermore, $Cr(CN)_6$ is suitable, whereas $Co(CN)_6$ is not, as a cyanide-centered PBA metal for use as a pressure-induced water production material. Regarding the reusability of the CuCr PBA, even after exposure to high humidity for several hours (80% RH for 4 h), the material did not easily reabsorb water. However, when the CuCr PBA was immersed in water, the IR spectra indicated that this material readily reabsorbed water. The application of pressure to the CuCr PBA that had reabsorbed water lowered the intensity of the IR peak of water, indicating the potential for reusability via immersion in water. However, further optimisation of the experimental conditions using a trial-and-error approach combined with validation would be necessary to confirm practical reusability.

The present work provides insights into the design of pressure-induced water production materials, which require the following three characteristics. (i) The crystal structure must contain pores capable of accommodating water; (ii) the crystal framework should be maintained under pressure; (iii) the pores that accommodate the water must become hydrophobic upon the application of pressure. The first two characteristics are satisfied by numerous reported materials, such as porous metal-organic frameworks. Imparting the functionality described in (iii) to materials presents a significant challenge in the design and development of materials that exhibit pressure-induced water production. In the case of the CuCr PBA studied in this work, the application of pressure induced partial electron transfer between Cu and O led to the hydrophobisation of the pores.

Water production in arid regions remains an urgent global challenge. Proposing a method in which water is produced by applying pressure represents a significant advancement in water production technologies for operation under diverse environmental conditions, beyond those based solely on temperature and humidity controls. Inducing temperature or humidity variations artificially requires specialized equipment such as temperature/humidity regulators and an external energy source. Moreover, using natural environmental changes often involves prolonged waiting periods and can be challenging owing to fluctuating conditions. In contrast, pressure variations can be manually induced using simple equipment such as a press, yielding immediate results less susceptible to external influences. As a separate point, Prussian blue analogs, with their three-dimensional rigid open framework and high theoretical specific capacity, are promising electrode materials for sodium-ion batteries.[53,54] However, defects and coordinated water molecules generated during synthesis negatively affect their electrochemical properties.[55,56] This study presents a mechanical method to apply pressure and release water, potentially reducing water content and enhancing electrochemical performance.[57,58] This approach shows potential as a complementary method for enhancing energy storage applications.

Author contributions

Please refer to the ESI for details.

Acknowledgements

This research was supported in part by the Japan Science and Technology FOREST Program (JPMJFR213Q), Japan Society for the Promotion of Science Grant-in-Aid for Scientific Research (B) (22H02046), the JST SPRING program (JSMJSP2124), and Tsukuba Basic Research Support Program (Type S). Synchrotron experiments were carried out as joint research by the Synchrotron Radiation Research Organization and Institute for Solid State Physics, The University of Tokyo (Proposal Number 2017A7535). We are grateful to Prof. Asuka Namai for her technical support. We acknowledge the support of the Cryogenic Research Center and Center for Nano Lithography & Analysis at The University of Tokyo, which are supported by MEXT.

Conflicts of interest

There are no conflicts to declare.

Data availability

The data supporting this article are included as part of ESI.

Notes and references

1 E. Coronado, Molecular magnetism: from chemical design to spin control in molecules, materials, and devices *Nat. Rev. Mater.*, 2020, **5**, 87–104.

2 S. Ohkoshi, K. Nakagawa, K. Imoto, H. Tokoro, Y. Shibata, K. Okamoto, Y. Miyamoto, M. Komine, M. Yoshikiyo and A. Namai, A photoswitchable polar crystal that exhibits superionic conduction, *Nat. Chem.*, 2020, **12**, 338–344.

3 S. F. Jafri, E. S. Koumousi, M. -A. Arrio, A. Juhin, D. Mitcov, M. Rouzieres, P. Dechambenoit, D. Li, E. Otero, F. Wilhelm, A. Rogalev, L. Joly, J. -P. Kappler, C. C. D. Moulin, C. Mathonière, R. Clérac and P. Sainctavit, Atomic-scale evidence of the switching mechanism in a Photomagnetic CoFe dinuclear Prussian blue analogue, *J. Am. Chem. Soc.*, 2019, **141**, 3470–3479.

4 M. Magott, M. Reczynski, B. Gawel, B. Sieklucka and D. Pinkowicz, A Photomagnetic Sponge: High-Temperature Light-Induced Ferrimagnet Controlled by Water Sorption, *J. Am. Chem. Soc.*, 2018, **140**, 15876–15882.

5 N. Hoshino, F. Iijima, G. N. Newton, N. Yoshida, T. Shiga, H. Nojiri, A. Nakao, R. Kumai, Y. Murakami and H. Oshio, Three-way switching in a cyanide-bridged [CoFe] chain, *Nat. Chem.*, 2012, **4**, 921–926.

6 S. S. Kaye and J. R. Long, Hydrogen Storage in the Dehydrated Prussian Blue Analogues $M_3[Co(CN)_6]_2$ (M = Mn, Fe, Co, Ni, Cu, Zn), *J. Am. Chem. Soc.*, 2005, **127**, 6506–6507.

7 S. Ohkoshi, K. Nakagawa, K. Tomono, K. Imoto, Y. Tsunobuchi and H. Tokoro, High Proton Conductivity in Prussian Blue Analogs and the Interference Effect by Magnetic Ordering, *J. Am. Chem. Soc.*, 2010, **132**, 6620–6621.
8 S. Ferlay, T. Mallah, R. Ouahès, P. Veillet and M. Verdaguer, A Room-Temperature Organometallic Magnet Based on Prussian Blue, *Nature*, 1995, **378**, 701–703.
9 W. E. Buschmann, S. C. Paulson, C. M. Wynn, M. A. Girtu, A. J. Epstein, H. S. White and J. S. Miller, Magnetic field-induced reversed (negative) magnetization for electrochemically deposited T_C = 260 K oxidised films of chromium cyanide magnets, *Adv. Mater.* 1997, **9**, 645–647.
10 H. Tokoro and S. Ohkoshi, Multifunctional material: bistable metal-cyanide polymer of rubidium manganese hexacyanoferrate, *Bull. Chem. Soc. Jpn.*, 2015, **88**, 227–239.
11 A. Bleuzen, C. Lomenech, V. Escax, F. Villain, F. Varret, C. C. D. Moulin and M. Verdaguer, Photoinduced Ferrimagnetic Systems in Prussian Blue Analogues $C^{I}_{x}Co_4[Fe(CN)_6]_y$ (C^{I} = Alkali Cation). 1. Conditions to observe the Phenomenon, *J. Am. Chem. Soc.,* 2000, **122**, 6648–6652.
12 S. Ohkoshi, K. Arai, Y. Sato and K. Hashimoto, Humidity-induced magnetisation and magnetic pole inversion in a cyano-bridged metal assembly, *Nat. Mater.*, 2004, **3**, 857–861.
13 H. Tokoro, T. Matsuda, T. Nuida, Y. Moritomo, K. Ohoyama, E. D. L. Dangui, K. Boukheddaden and S. Ohkoshi, Visible-Light-Induced Reversible Photomagnetism in Rubidium Manganese Hexacyanoferrate, *Chem. Mater.*, 2008, **20**, 423–428.
14 S. Pintado, S. Goberna-Ferron, E. C. Escudero-Adan and J. R. Galan-Mascaros, Fast and Persistent Electrocatalytic Water Oxidation by Co-Fe Prussian Blue Coordination Polymers, *J. Am. Chem. Soc.*, 2013, **135**, 13270–13273.
15 Y. H. Lu, L. Wang, J. G. Cheng and J. B. Goodenough, Prussian blue: A new framework of electrode materials for sodium batteries, *Chem Commun.*, 2012, **48**, 6544–6546.
16 H. W. Lee, R. Y. Wang, M. Pasta, S. W. Lee, N. Liu and Y. Cui, Manganese hexacyanomanganate open framework as a high-capacity positive electrode material for sodium-ion batteries, *Nat. Commun.*, 2014, **5**, 5280.
17 L. Han, X. Y. Yu and X. W. Lou, Formation of Prussian-Blue-Analogue Nanocages via a Direct Etching Method and their Conversion into Ni-Co-Mixed Oxide for Enhanced Oxygen Evolution, *Adv. Mater.*, 2016, **28**, 4601–4605.
18 W. Wang, Y. Gang, Z. Hu, Z. Yan, W. Li, Y. Li, Q. -F. Gu, Z. Wang, S. -L. Chou, H. -K. Liu and S. -W. Dou, Reversible structural evolution of sodium-rich rhombohedral Prussian blue for sodium-ion batteries, *Nat. Commun.*, 2020, **11**, 980.
19 P. Gutlich, Y. Garcia and T. Woike, Photoswitchable Coordination Compounds, *Coord. Chem. Rev.*, 2001, **219**, 839–879.
20 S. Ohkoshi and H. Tokoro, Photomagnetism in Cyano-Bridged Bimetal Assemblies, *Acc. Chem. Res.*, 2012, **45**, 1749–1758.
21 A. C. Felts, A. Slimani, J. M. Cain, M. J. Andrus, A. R. Ahir, K. A. Abboud, M. W. Meisel, K. Boukheddaden and D. R. Talham, Control of the Speed of a Light-Induced Spin Transition through Mesoscale Core-Shell Architecture, *J. Am. Chem. Soc.*, 2018, **140,** 5814–5824.
22 H. Tokoro, A. Namai, M. Yoshikiyo, R. Fujiwara, K. Chiba and S. Ohkoshi, Theoretical prediction of charge-transfer phase transition, *Sci. Rep.*, 2018, **8**, 63.
23 S. Nagashima, Y. Yahagi, M. Nishino, T. Yamaoka, K. Nakagawa, J. Wang, S. Ohkoshi and H. Tokoro, Direct Observation of Magnetic Domain and Magnetization Reversal on Prussian Blue-Based Magnetic Films, *J. Am. Chem. Soc.*, 2023, **145**, 22934–22944.
24 M. Cammarata, S. Zerdane, L. Balducci, G. Azzolina, S. Mazerat, C. Exertier, M. Trabuco, M. Levantino, R. Alonso-Mori, J. M. Glownia, S. Song, L. Catala, T. Mallah, S. F. Matar and E. Collet, Charge transfer driven by ultrafast spin transition in a CoFe Prussian blue analogue, *Nat. Chem.*, 2021, **13**, 10–14.
25 M. Verdaguer, A. Bleuzen, V. Marvaud, J. Vaissermann, M. Seuleiman, C. Desplanches, A. Scuiller, C. Train, R. Garde, G. Gelly, C. Lomenech, I. Rosenman, P. Veillet, C. Cartier and F. Villain, Molecules to build solids: high T_C molecule-based magnets by design and recent revival of cyano complexes chemistry. *Coord. Chem. Rev.*, 1999, **190–192**, 1023–1047.
26 H. Tokoro and S. Ohkoshi, Novel magnetic functionalities of Prussian blue analogues, *Dalton Trans.,* 2011, **40**, 6825–6833.
27 P. Dechambenoit and J. R. Long, Microporous magnets, *Chem. Soc. Rev.*, 2011, **40**, 3249–3265.
28 X. -Y. Wang, C. Avendano and K. R. Dunbar, Molecular magnetic materials based on 4d and 5d transition metals, *Chem. Soc. Rev.*, 2011, **40**, 3213–3238.
29 E. Coronado and G. M. Espallargas, Dynamic magnetic MOFs, *Chem. Soc. Rev.*, 2013, **42**, 1525–1539.
30 H. Tokoro and S. Ohkoshi, Multifunctional material: bistable metal-cyanide polymer of rubidium manganese hexanoferrate, *Bull. Chem. Soc. Jpn.*, 2015, **88**, 227–239.
31 M. Ishizaki, S. Akiba, A. Ohtani, Y. Hoshi, K. Ono, M. Matsuba, T. Togashi, K. Kananizuka, M. Sakamoto, A. Takahashi, T. Kawamoto, H. Tanaka, M. Watanabe, M. Arisaka, T. Nankawa and M. Kurihara, Proton-exchange mechanism of specific Cs+ adsorption via lattice defect sites of Prussian blue filled with coordination and crystallization water molecules, *Dalton Trans.*, 2013, **42**, 16049–16055.
32 S. Ohkoshi, M. Yoshikiyo, A. Namai, K. Nakagawa, K. Chiba, R. Fujiwara and H. Tokoro, Cesium ion detection by terahertz light, *Sci. Rep.*, 2017, **7**, 8088.
33 A. Takahashi, H. Tanaka, D. Parajuli, T. Nakamura, K. Minami, Y. Sugiyama, Y. Hakuta, S. Ohkoshi and T. Kawamoto, Historical Pigment Exhibiting Ammonia Gas capture beyond Standard Adsorbents with Adsorption Sites of Two Kinds, *J. Am. Chem. Soc.*, 2016, **138**, 6376–6379.
34 K. Itaya, K. Shibayama, H. Akahoshi and S. Toshima, Prussian-blue-modified electrodes: An application for a stable electrochromic display device, *J. Appl. Phys.*, 1982, **53**, 804–805.
35 A. Paolella, C. Faure, V. Timoshevskii, S. Marras, G. Bertoni, A. Guerfi, A. Vijh, M. Armand and K. Zaghib, A review on hexacyanoferrate-based materials for energy storage and smart windows: challenges and perspectives, *J. Mater. Chem. A*, 2017, **5**, 18919–18932.
36 A. Ludi, H. U. Güdel and M. Ruegg, The structural chemistry of Prussian blue analogs. single-crystal study of manganese(II) hexacyanocobaltate(III), $Mn_3[Co(CN)_6]_2{\cdot}xH_2O$. *Inorg. Chem.*, 1970, **9**, 2224–2227.
37 F. Herren, P. Fischer, A. Ludi and W. Hälg, Neutron Diffraction Study of Prussian Blue, $Fe_4[Fe(CN)_6]_3{\cdot}xH_2O$. Location of Water Molecules and Long-Range Magnetic Order. *Inorg. Chem.*, 1980, **19**, 956–959.
38 A. Simonov, T. D. Baerdemaeker, H. L. B. Boström, M. L. R. Gómez, H. J. Gray, D. Chernyshov, A. Bosak, H. -B. Bürgi and A. L. Goodwin, Hidden diversity of vacancy networks in Prussian blue analogues, *Nature*, 2020, **578**, 256–260.
39 M. M. Mekonnen and A. Y. Hoekstra, Four billion people facing severe water scarcity, *Sci. Adv.*, 2016, **2**, e1500323.
40 Y. Guo, J. Bae, Z. Fang, P. Li, F. Zhao and G. Yu, Hydrogels and Hydrogel-Derived Materials for Energy and Water Sustainability, *Chem. Rev.*, 2020, **120**, 7642–7707.
41 T. Xu, X. Ding, H. Cheng, G. Han and L. Qu, Moisture-Enabled Electricity from Hygroscopic Materials: A New Type of Clean Energy, *Adv. Mater.*, 2023, 2209661.

42 N. Hanikel, X. Pei, S. Chheda, H. Lyu, W. S. Jeong, J. Sauer, L. Gagliardi and O. M. Yaghi, Evolution of water structures in metal-organic frameworks for improved atmospheric water harvesting, *Science*, 2021, **374**, 454–459.

43 J. Xu, T. Li, J. Chao, S. Wu, T. Yan, W. Li, B. Cao and R. Wang, Efficient Solar-Driven Water Harvesting from Arid Air with Metal-Organic Frameworks Modified by Hygroscopic Salt, *Angew. Chem. Int. Ed.*, 2020, **59**, 5202–5210.

44 D. F. Shriver, S. A. Shriver and S. E. Anderson, Ligand Field Strength of Nitrogen End of Cyanide and Structures of Cubic Cyanide Polymers, *Inorg. Chem.*, 1965, **4**, 725–730.

45 W. E. Buschmann, J. Ensling, P. Gutlich and J. S. Miller, Electron Transfer, Linkage Isomerization, Bulk Magnetic Order, and Spin-Glass Behavior in the Iron Hexacyanomanganate Prussian Blue Analogue, *Chem. Eur. J.*, 1999, **5**, 3019-3028.

46 M. P. Shores, J. J. Sokol and J. R. Long, Nickel(II)-Molybdenum(III)-Cyanide Clusters: Synthesis and Magnetic Behavior of Species Incorporating $[(Me_3tacn)Mo(CN)_3]$, *J. Am. Chem. Soc.*, 2002, **124**, 2279–2292.

47 E. Coronado, M. C. Giménez-López, G. Levchenko, F. M. Romero, V. García-Baonza, A. Milner and M. Paz-Pasternak, Pressure-Tuning of Magnetism and Linkage Isomerism in Iron(II) Hexacyanochromate, *J. Am. Chem. Soc.*, 2005, **127**, 4580–4581.

48 P. Bhatt, N. Thakur, M. D. Mukadam, S. S. Meena and S. M. Yusuf, Evidence for the Existence of Oxygen Clustering and Understanding of Structural Disorder in Prussian Blue Analogues Molecular Magnet $M_{1.5}[Cr(CN)_6)]\cdot zH_2O$ (M = Fe and Co): Reverse Monte Carlo Simulation and Neutron Diffraction Study, *J. Phys. Chem. C*, 2013, **117**, 2676–2687.

49 W. -W. Wu, K. -P. Xie, G. -Z. Huang, Z. -Y. Ruan, Y. -C. Chen, S. -G. Wu, Z. -P. Ni and M. -L. Tong, Single-Crystal to Single-Crystal Transformation of a Spin-Crossover Hybrid Perovskite via Thermal-Induced Cyanide Linkage Isomerization, *Inorg. Chem.*, 2022, **61**, 9047–9054.

50 S. Myneni, Y. Luo, L.Å. Näslund, M. Cavalleri, L. Ojamäe, H. Ogasawara, A. Pelmenschikov, Ph. Wernet, P. Väterlein, C. Heske, Z. Hussain, L. G. M. Pettersson and A. Nilsson, Spectroscopic probing of local hydrogen-bonding structures in liquid water, *J Phys: Condens. Mat.*, 2002, **14**, L213–L219.

51 M. Grioni, J. F. van Acker, M. T. Czyžzyk and J. C. Fuggle, Unoccupied electronic structure and core-hole effects in the x-ray-absorption spectra of Cu_2O, *Phys. Rev. B*, 1992, **45**, 3309–3318.

52 J. P. Hu, D. J. Payne, R. G. Egdell, P. A. Glans, T. Learmonth, K. E. Smith, J. Guo and N. M. Harrison, On-site interband excitations in resonant inelastic x-ray scattering from Cu_2O, *Phys. Rev. B*, 2008, **77**, 155115.

53 B. Singh and A. Indra, Prussian blue- and Prussian blue analogue-derived materials: progress and prospects for electrochemical energy conversion, *Mater. Today Energy*, 2020, **16**, 100404.

54 H. Zhang, Y. Gao, J. Peng, Y. Fan, L. Zhao, L. Li, Y. Xiao, W. K. Pang, J. Wang and S. Chou, Prussian blue analogues with optimized crystal plane orientation and low crystal defects toward 450 Wh kg^{-1} alkali-ion batteries, *Angew. Chem. Int. Ed.*, 2023, **62**, e202303953.

55 L. Ge, Y. Song, P. Niu, B. Li, L. Zhou, W. Feng, C. Ma, X. Li, D. Kong, Z. Yan, Q. Xue, Y. Cui and W. Xing, Elaborating the Crystal water of prussian blue for outstanding performance of sodium ion batteries, *ACS Nano*, 2024, **18**, 3542–3552.

56 D. Yang, J. Xu, X.-Z. Liao, H. Wang, Y.-S. He and Z.-F. Ma, Prussian blue/RGO with less coordinated water as superior cathode material for sodium-ion batteries, *Chem. Commun.*, 2023, **59**, 211–214.

57 H. L. B. Boström, I. E. Collings, D. Daisenberger, C. J. Ridley, N. P. Funnell and A. B. Cairns, Probing the influence of defects, hydration, and composition on prussian blue analogues with pressure, *J. Am. Chem. Soc.*, 2021, **143**, 3544 −3554.

58 M. Zentkova and M. Mihalik, The Effect of pressure on magnetic properties of prussian blue analogues, *Crystals*, 2019, **9**, 112.

Data availability statements

"Pressure-induced water producing using a copper–chromium Prussian blue analog"

by Shintaro Akagi, Mayuko Tanaka, Junhao Wang, Hisao Kiuchi, Yoshihisa Harada, Yizhou Chen, Kazuhiro Marumoto, Kenta Imoto, Shin-ichi Ohkoshi, Hiroko Tokoro

The data supporting this article are included as part of Electronic Supplementary Information (ESI).